GPS Solutions (2024) 28:84
https://doi.org/10.1007/s10291-023-01606-2

ORIGINAL ARTICLE

A modified adaptive factor-based Kalman filter for continuous urban navigation with low-cost sensors

Sudha Vana[1,2] · **Sunil Bisnath**[1]

Received: 23 July 2023 / Accepted: 21 December 2023 / Published online: 13 March 2024

Abstract

Low-cost sensor navigation has risen in the past decade with the onset of many modern applications that demand decimeter-level accuracy using mass-market sensors. The key advantage of the precise pointing positioning (PPP) technique over real-time kinematic (RTK) is the non-requirement of local infrastructure and still being able to attain decimeter to sub-meter level accuracy while using mass-market low-cost sensors. Achieving decimeter to sub-meter-level accuracy is a challenge in urban environments. Therefore, adaptive filtering for low-cost sensors is necessary along with motion-based constraining and atmosphere constraints. The traditional robust adaptive Kalman filter (RAKF) uses empirical limits that are derived by analyzing the GNSS receiver data learning statistics based on confidence intervals beforehand to determine when the adaptive factor needs to be applied. In this research, a new technique is proposed to determine the adaptive factor computation based on the detection of an increase in the number of satellite signals after a partial outage. The proposed method provides 6–46% better accuracy than the traditional RAKF and 11–55% better accuracy performance when compared to a tightly coupled solution without enhancements when multiple datasets were tested. The results prove to be a significant improvement for the next generation of applications, such as low-autonomous and intelligent transportation systems.

Keywords GNSS · Precise point positioning · IMU · Kalman filtering · Low-cost navigation · Urban navigation

Introduction

The emergence of new applications such as autonomous vehicles, navigation using smart devices, intelligent transportation systems and other modern applications, the demand for accurate and continuous navigation has skyrocketed. In urban areas, using high-quality global navigation satellite system (GNSS) and inertial measurement unit (IMU) sensors with the real-time kinematic (RTK) or precise point positioning (PPP) GNSS measurement processing techniques might be able to offer sub-meter to decimeter-level accuracy. With the recent advancement in hardware technology and software, modern applications require decimeter to sub-meter level accuracy using low-cost sensors. Achieving decimeter-level accuracy using low-cost sensors is a greater challenge, as the quality of measurements is poor when the GNSS signal reception environment is obstructed (Vana 2023; Vana and Bisnath 2020).

The main advantages of the PPP technique when compared to RTK technique are (Choy et al. 2016; Zumberge et al. 1997): 1. the non-requirement of local ground-based infrastructure and usage of the precise products to obtain a precise and accurate position solution; and 2. provision of point positioning information. These reasons make PPP a very desirable alternative to RTK/relative positioning. The disadvantage of using PPP is the long convergence time; it takes 10–15 min to achieve a cm level accuracy in stationary mode. Various techniques are used to decrease PPP convergence time, such as adding more GNSS measurements, constraining the ionospheric delay's estimation using global ionospheric maps (GIMs), ambiguity resolution, sensor integration, etc.

In a standard EKF, the assumption made is that the dynamic model constructed is ideal for the application's environment (Brown and Hwang 1997). However, the application environment is a factor that cannot be held as a constant, given the type of applications targeted by this

✉ Sudha Vana
vana.sudha@gmail.com

[1] Department of Earth and Space Science and Engineering, York University, Toronto, ON M3J1P3, Canada

[2] Rx Networks, Vancouver, BC V6E2V2, Canada

work, which are low-cost autonomous and intelligent transportation systems, virtual reality, etc. Adaptive filtering is mandatory to serve such requirements. Some of the common adaptive filters are innovation-based adaptive estimation (IAE) (Hide et al. 2003), multiple-model adaptive estimation (MMAE) (Magill 1965) and robust adaptive KF (RAKF) (Yang and Cui 2008; Zhou et al. 2009). IAE method that uses past information can introduce unnecessary large errors in the solution due to larger solution errors from past data. In the case of MMAE, running multiple parallel filters causes processing overhead to the system. Therefore, in this work, RAKF has been explored.

The adaptability in the RAKF algorithm comes in two stages. In the first phase, an equivalent measurement covariance matrix is formed with the help of a standardized residual statistic. In the second phase, an adaptive factor is introduced to balance the contributions of predicted states, in this case, the IMU-based prediction and new measurements from the current epoch are observed. The traditional RAKF uses empirical values derived from confidence intervals to compute the equivalent measurement covariance matrix and the adaptive factor. Only the adaptive factor portion for the dynamic model is explored in this research work.

In the past, Yang and Gao (2005) conducted a study comparing different types of adaptive factors with different segments such as 2- and 3-segment adaptive factor functions. In the experiments conducted by Yang and Gao (2005), a Trimble 4500 receiver was used in RTK mode and produced double-differenced carrier-phase measurements. The adaptive function used to compare the results was the state discrepancy-based method. The results from Yang and Gao (2005) claim 60% better horizontal accuracy performance when compared to traditional EKF.

Recent studies such as Elmezayen and El-Rabbany (2021) and Lotfy et al. (2022) working on RAKF focus on adaptive observation models for a specific set of observations, such as adaptiveness applied to observations from a particular frequency or constellation. The traditional RAKF model has been adapted by using a classification robust adaptive Kalman filter (CAKF). In a CAKF, an equivalent weight function model based on a t-test statistic is formed, and an equivalent weight matrix for different types of observations (e.g., $P1$, $L1$, $P2$, $L2$, etc.) is developed separately. Results from these studies claim accuracy improvement of about 15–45%.

In Wu et al. (2022), both measurement adaptiveness and predicted state covariance adaptiveness are employed using GNSS and IMU tightly coupled (TC) integration with RAKF. For predicted state covariance adaptive factor calculation, the PDOP value is used as an indicator to apply the adaptation computation. The learning statistic used in this research is based on standardized residuals. The experiments were conducted using a Leica GNSS Gx 1230 and CMIGITS-II IMU in an open-sky environment and areas covered with foliage. The authors summarized that when the proposed method was observed, the horizontal solution error was 31% superior when compared to the standard extended Kalman filter (EKF).

In the study conducted by Li and Shen (2011), TC integration of GPS and IMU measurements was performed using a trimble GPS and a tactical grade IMU for an aerial object using the double-differencing method by placing a reference station at a known location. As part of the case study, simulated noise was introduced on code measurements and the RAKF with measurement adaptiveness maintained an RMS of 70 cm, while the RAKF with both measurement and dynamic model adaptiveness achieved an RMS of 60 cm when compared to a standard EKF with an RMS of a couple of meters. In the latter part, abnormal noises were added to the IMU measurements and the RAKF with both measurement as well as dynamic model adaptability remained at 60 cm, while standard EKF and RAKF with just measurement adaptability, had a poor performance with an RMS of 10 m.

A modified-RAKF is proposed in this work by trying to detangle the dependence of the RAKF application using empirical cutoff values that are derived based on a hypothesis test. The method relies on the fact that large errors in the estimation process occur when new satellites are acquired after a partial outage (i.e., in the urban area case). Therefore, the method works by detecting new satellites and then applying the RAKF, rather than applying various statistical Yang and Cui (2008) and Yang and Gao (2005). The objectives of this work are to 1. Evaluate the accuracy performance of low-cost navigation system by applying modified-RAKF adaptive factors in urban environments 2. Assess and compare two different learning statistics. This section is followed by an introduction to GNSS-PPP and IMU integration and the existing adaptive filters, followed by modified-RAKF, field test results, and conclusions and recommendations.

GNSS-PPP and IMU integration

In this research, triple-frequency (TF) GNSS measurements are processed in uncombined mode. When all three frequency measurements are available for a satellite, the measurements are processed in TF mode and when only two frequency measurements are available, the measurements are processed in dual-frequency (DF) mode. The code and carrier-phase measurements can be expressed as shown below (Hofmann-Wellenhof et al. 2007; Naciri and Bisnath 2021).

$$P_i^s = \rho + c\left(\mathrm{d}t_\mathrm{r} - \mathrm{d}t^s\right) + T + \gamma_i I_i^s + \left(B_p^r - B_p^s\right) + e_P \tag{1}$$

$$\varphi_i^s = \rho + c\left(\mathrm{d}t_\mathrm{r} - \mathrm{d}t^s\right) + T - \gamma_i I_i^s + \lambda_i^s\left(N_i + B_\varphi^r - B_\varphi^s\right) + e_\varphi \tag{2}$$

In (1) and (2), s represents a satellite, $i = 1, 2$ and 5 represent the first, second and third signal frequencies, ρ is the geometric range between a satellite and the user position, dt_r is the receiver clock errors, dt_s is the satellite clock error, T is the troposphere delay, $\gamma_i = \frac{f_i^2}{f_1^2}$ is the ratio of frequencies applied to the first frequency ionosphere delay I_i^s at frequency i, B_p^r and B_p^s are the receiver and satellite hardware biases, respectively, B_φ^r and B_φ^s are the receiver and satellite phase biases, respectively, and e_P and e_φ represent the receiver noise and multipath, respectively. The ionosphere state per satellite is estimated as white noise and constrained using GIM. $\lambda_i^s = c/f_i$ is the signal wavelength per satellite and N_i is the integer ambiguity on each frequency (Vana 2023). The details of ionospheric constraining can be found in Aggrey (2018), Cai et al. (2017), Vana (2023) and Yi et al. (2021).

An elevation-based weighting scheme is used for the measurements which is improvised from Eueler and Goad (1991). Further system and measurement modeling details can be found in Vana (2023).

Figure 1 is a representation of TC integration block diagram of GNSS-PPP and MEMS-IMU measurements. The TF-GNSS measurements are corrected for the orbit, clock and biases using the precise corrections obtained from analysis centers. Further, the measurements are corrected for the earth rotation, atmosphere, relativistic and phase wind-up corrections as well. The corrected code and phase measurements are represented by ρ_{GNSS} and φ_{GNSS}, respectively.

f_b and w_b are the specific force and turn rates, respectively, measured by the MEMS-IMU which are converted into position (P_{IMU}), velocity (V_{IMU}) and attitude (A_{IMU}) by using inertial mechanization. The details of inertial mechanization can be found in references such as Farrell (2008) and Groves (2013). Using the satellite positions and position P_{IMU}, predicted code and phase observations are obtained which are represented by (ρ_{IMU} and φ_{IMU}). The input to the EKF is the residuals between the GNSS measurements and the predicted IMU measurements. Integer ambiguities are not resolved and estimated as float since the applications targeted by this research do not require centimeter level accuracy. The error states δP, δv, $\delta \epsilon$, δb_a and δb_g are fed back to inertial mechanization. P_{IMU}^e, V_{IMU}^e and A_{IMU}^e are the corrected IMU position, velocity and attitude. Motion constraining or non-holonomic constraining (NHC) is applied to the IMU measurements based on vehicle dynamics. The details of the vehicle dynamics applied can be found in Vana (2023) and Vana et al. (2020).

Robust adaptive Kalman filter

A robust adaptive Kalman filter (RAKF) was developed by combining adaptive filtering and robust estimation theory. RAKF is adopted to avoid abnormal measurements in difficult environments for measurement collection (Yang et al. 2001; Yang and Cui 2008; Yang and Gao 2006). For example, while using GNSS in difficult environments such as an urban area, the system model may vary with time (Niehsen 2004). To balance the contributions of observations and predicted states to estimated state parameters, the robust adaptive factor α is set as a piecewise decreasing function. The adaptive factor is computed based on learning statistics. Therefore, the function used for computing the adaptive factor needs to be chosen such that the abnormality in the observations is flagged using the learning statistic. In

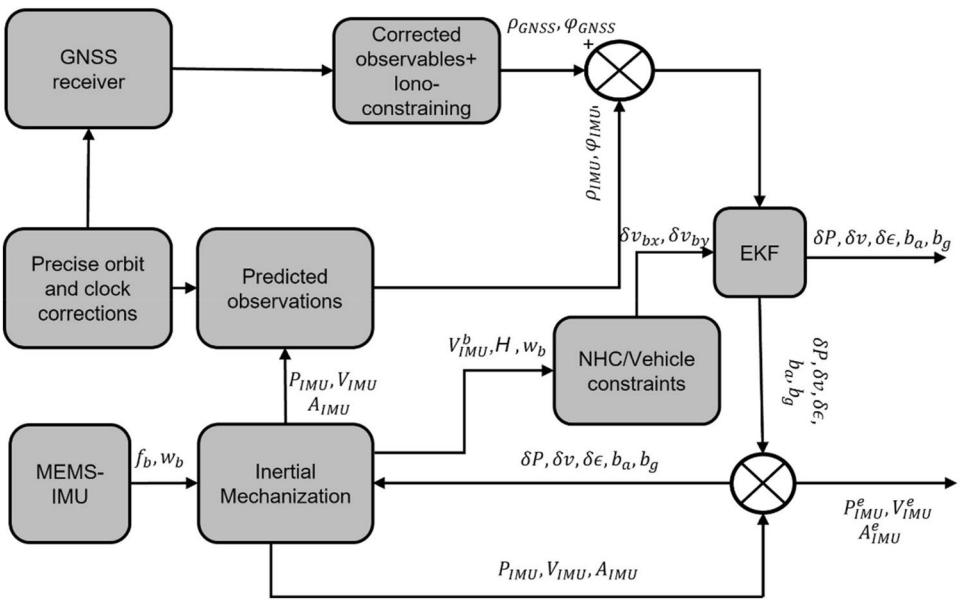

Fig. 1 GNSS-PPP MEMS-IMU TC integration diagram (Vana 2023)

this case, the adaptive factor is adjusted to trust more in the predicted states and vice versa.

The adaptive factor α is applied to the Kalman gain by scaling the predicted state covariance as shown below.

$$\tilde{K}_k = \alpha_k P_k^- H_k^T \left[\alpha H_k P_k^- H_k^T + R_k\right]^{-1} \tag{3}$$

$$\tilde{P}_k = \left[I - \tilde{K}_k H_k\right] P_k^- \left[I - \tilde{K}_k H_k\right]^{\mathrm{T}} + \tilde{K}_k R_k \tilde{K}_k^{\mathrm{T}} \tag{4}$$

In (3) and (4), P_k^- is the predicted state covariance, H_k is the design matrix, and R_k is the measurement covariance.

Different methods can be used to compute the adaptive factor α, centered on the learning statistic. The learning statistic can be computed using various statistical data that are available during the estimation process. Yang & Gao (2005) list various methods from the literature. The parameters used in this work are enlisted in Table 1.

Modified robust adaptive Kalman filter

The drawbacks of the traditional RAKF are: 1) the detection of the time period when the RAKF should be applied, 2) the computation of the adaptive factor depends on empirical values, and 3) the computation of correct measurement covariance adaptiveness in difficult environments. Using empirical values derived from hypothesis testing makes the technique more dependent on the measurement quality and the types of sensors used. The empirical values are typically derived by assessing multiple datasets for a particular sensor. This work aims to detach the dependence on empirical values that are derived using confidence intervals of the learning statistics while using the RAKF and make the computation process more independent of the measurement quality analysis for each sensor.

Before explaining the modified-RAKF (MRAKF), the accuracy performance of single point positioning (SPP), GNSS-PPP and GNSS-PPP + IMU is compared to understand when and how using RAKF can help in improving the navigation solution accuracy. Data collected on August 10,

Table 1 Learning statistics used in this work (Yang and Cui 2008; Yang and Gao 2006)

Learning statistic	Equation	Explanation of terms
Ratio of variance component using change in position and system innovations	$\left\lvert \Delta\overline{V}_k \right\rvert = \frac{\sigma_{0X}}{\sigma_{0k}}$ $\sigma_{0X} = \sqrt{\frac{\Delta\overline{X}_k^T P_{\overline{X}_k} \Delta\overline{X}_k}{m_k - \mathrm{tr}\left(N^{-1} P_{\overline{X}_k}\right)}}$ $\sigma_{0k} = \sqrt{\frac{V_k^T P_k V_k}{n_k - \mathrm{tr}\left(N^{-1} N_k\right)}}$	$\Delta\overline{X}_k$ = difference between the predicted and estimated position states $P_{\overline{X}_k}$ = post-fit covariance of position co-ordinates V_k = system innovations P_k = system innovations covariance m_k = number of predicted parameters of state vector n_k = number of measurements at an epoch $N_k = H_k^T P_k H_k$ $N = N_k + P_{\overline{X}_k}$ H_k is the design matrix
System innovations	$\left\lvert \Delta\overline{V}_k \right\rvert = \sqrt{\frac{V_k^T P_k V_k}{n_k - tr\left(N^{-1} N_k\right)}}$	$\left\lvert \Delta\overline{V}_k \right\rvert$ is the learning statistic computed using system innovations V_k = system innovations P_k = system innovations covariance n_k = number of measurements at an epoch $N_k = H_k^T P_k H_k$ $N = N_k + P_{\overline{X}_k}$ H_k is the design matrix

2022 including open-sky and urban areas at York University, Toronto, Canada, have been considered for the analysis. Septentrio Mosaic ×5 multi-frequency and multi-constellation GNSS receiver was used. The IMU used is the XSens MTi7, an industrial-grade MEMS-IMU. To compute the reference solution, a pair of NovAtel PwrPak 7 receivers and geodetic antennas (NOV-850) were set up, one as base and the other as rover. The experimental setup is as depicted in Fig. 2. The box with equipment was placed on car roof and driven. Data from the PwrPak7 receivers were post-processed using the Inertial Explorer software tool in smoothed RTK-TC mode.

Figure 3 represents the horizontal solution accuracy of SPP, GNSS-PPP only and PPP + IMU mode of processing the data. SPP solution accuracy also is presented in this comparison as some applications, such as many in the automotive industry, use the SPP solution as a standard. The SPP solution is produced by post-processing the Mosaic- ×5 data in the RTKlib processing tool. As seen in Fig. 3, the noisy nature of the SPP solution comes from the epoch-by-epoch least squares that do not carry the information from the past epochs to the current epoch. Also, the SPP solution uses single-frequency measurements and cannot accurately estimate the ionospheric refraction. GNSS-PPP and GNSS-PPP + IMU solutions are smoother than those from SPP because they are processed in a sequential least-squares filter and EKF, respectively. The GNSS-PPP and IMU measurements are fused in TC mode. As multi-frequency measurements are used, mitigation of ionosphere refraction is possible. The GNSS-PPP and GNSS-PPP + IMU solutions were processed using the York-PPP software in TF mode. The GNSS-PPP solution jumps whenever there is a drop in the number of satellites, causing an about 8 m level maximum spike in the position solution.

(a) Sensor box setup on the car roof

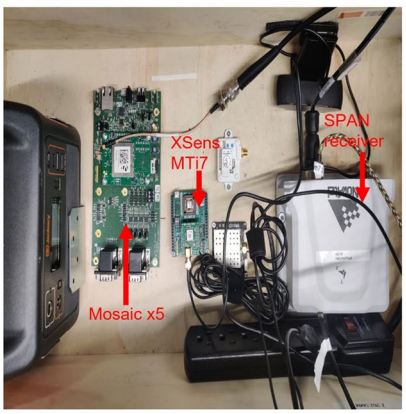

(b) View of the sensors inside the sensor box

(c) Test environment view

Fig. 2 Experimental setup and environment (Vana 2023)

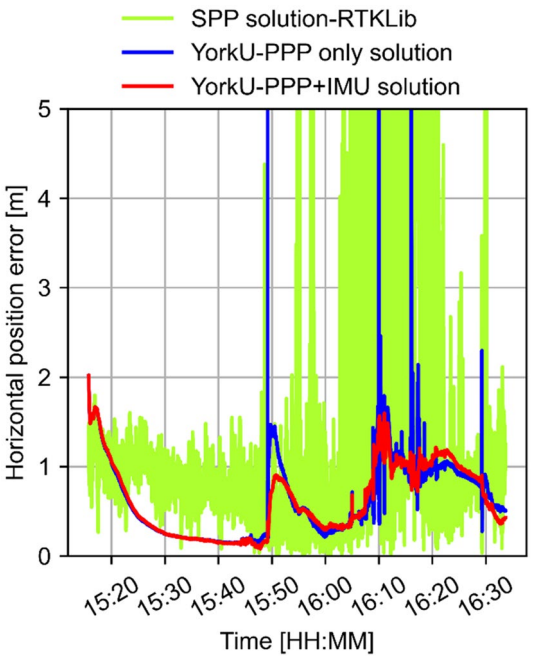

Fig. 3 Horizontal error plot of SPP-RTKLib, York-PPP and York-PPP + IMU

Table 2 Error statistics of the horizontal error of SPP-RTKLib, York-PPP and York-PPP + IMU

	SPP—RTKLib	PPP only	PPP + IMU
Horizontal RMS [m]	18	0.85	0.77
Horizontal RMS 95th percentile [m]	14.7	1.5	1.1
Maximum error [m]	37.2	8.2	2.1

Table 2 is a representation of the overall horizontal error RMS, horizontal RMS error 95th percentile and maximum error for all three processing techniques. The maximum horizontal error in the position solution progressively decreases, starting with SPP at 37 m to PPP + IMU at 2 m. The maximum position error for each of the three position solutions are also indicated in Table 2 to show the degree to which a solution can diverge during poor DOP or partial outages. These statistics indicate that integrating an IMU helps to minimize horizontal error in an urban environment.

In this research, an alternative method of using a RAKF is proposed by using the re-acquisition of satellite information to make the algorithm more independent of conducting a hypothetical test. The overview of the proposed MRAKF algorithm is shown in Fig. 4.

The step-by-step description and explanation of the proposed algorithm is as given below.

1. The correlation between the position error and the trend of satellites appearing and disappearing in an urban area was studied. When the number of satellites decreases, sub-meter or better accuracy is maintained by IMU mechanization. However, an increase in the position error typically occurs when satellites are re-acquired after traversing an underpass or between buildings. These new satellite signals acquired may be prone to multipath error, signal acquisition noise or a combination of both multipath and signal noise. Along with multipath affected measurements, the PPP algorithm takes time to converge causing spikes in the position solution. Another common problem is that when the vehicle passes multiple buildings in an urban area, DOP changes frequently. Therefore, to tackle this behavior/problem, the slope of the number of available satellites is recorded. The idea behind computing the slope of satellites being tracked is to detect the increasing satellite count, which will result in a positive slope. One second of data is used for estimating/detecting the slope, as the current data collection uses 5 Hz GNSS data and five samples/sec give a fair estimate of appearing and disappearing satellites. Also, less than one second may not give the true indication of satellites increasing or decreasing in an urban environment. Conversely, more than one second of data may delay the detection of post-outage situations. $y = mx + b$ represented in Fig. 4 is intercept-form of a straight line, where m is the slope of the line and b is the y-intercept. In this context, x vector represents time samples and y vector represents the number of satellites for the one second long data. To determine the slope, a linear regression is applied to the number of satellite information to estimate the slope parameters. If the slope is positive and if there are more states to be estimated than measurements, then the MRAKF algorithm is invoked. Figure 5 is a plot of the number of satellites in an urban area where the satellite count changes rapidly.

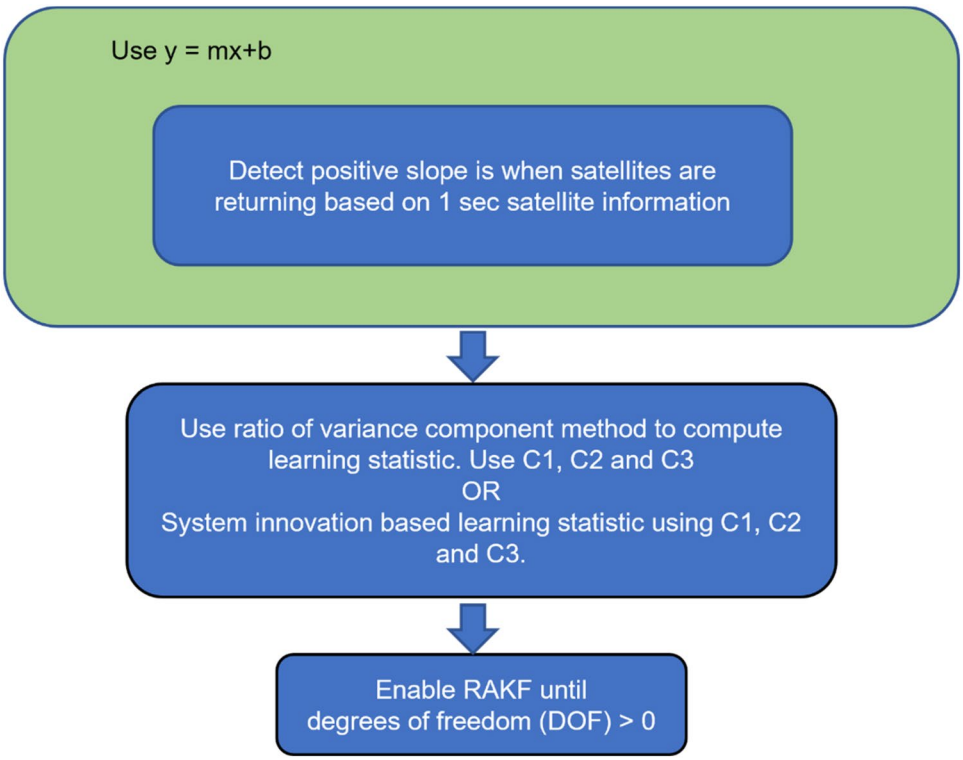

Fig. 4 Step-by step illustration of proposed modified-RAKF

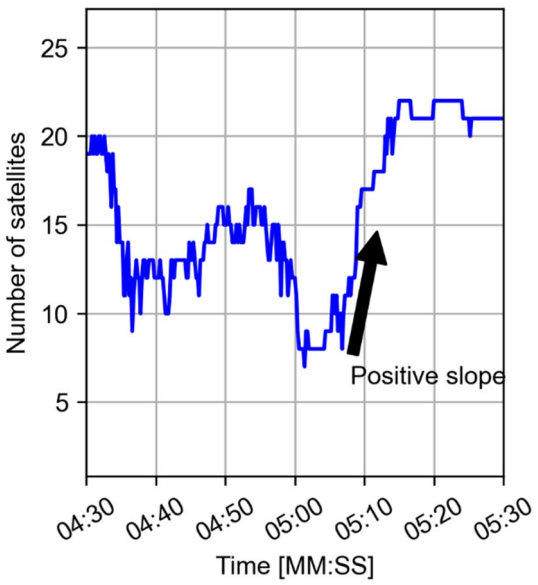

Fig. 5 Plot indicating positive slopes of satellites during signal re-acquisition post-outage (August 10, 2022)

2. Once the RAKF algorithm is invoked, the learning statistic is computed. As part of this research, two learning statistics were computed to compare performance: (1) variance component ratio and (2) system innovation. Table 1 describes the details of the two methods.
3. The next step is to compute the adaptive factor based on the learning statistic. In this research work, a two-segment adaptive factor was adopted. As the objective of this research is to apply the adaptive factor when the positive slope is detected, 2-segment adaptive factor function is suitable.

$$\alpha = \exp\left(-1 * \left|\Delta\overline{V}_k\right|\right) \tag{5}$$

Equation (5) shows the formula used for computing the adaptive factor α. $\left|\Delta\overline{V}_k\right|$ is the learning statistic (computed using variance component ratio method or the system innovation learning statistic method). In Fig. 4, $C1$, $C2$ and $C3$ represent the $L1$, $L2$ and L5 frequency pseudorange measurements, respectively.

$$\alpha = \begin{cases} 1 & \text{if Sl} \le 0 \text{ or DOF} > 0 \\ \exp\left(-1 * \left|\Delta\overline{V}_k\right|\right) & \text{if Sl} > 0 \end{cases} \tag{6}$$

The final two-segment adaptive factor method used can be represented by (6). It is important to note that (6) does not use any empirical values. In (6), Sl is the slope of the number of satellites for 1 s of data and DOF is degrees-of-freedom. Adaptive factor α is applied to the KF equations as shown in (3) and (4).

Field tests and results

Field tests were conducted to evaluate the positioning performance of the proposed MRAKF method. The sensors used and experimental setup are as described in Fig. 2.

Data collected on August 10, 2022 are discussed in this section followed by multiple datasets. York-PPP and IMU TC solutions were processed in simulated real-time mode with the same data to assess positioning performance. IMU motion constraining and ionosphere constraining for GNSS measurements were applied (Vana et al. 2020).

In order to study the observation errors in the collected Mosaic x5 data, double-differenced measurements were formed with the collocated geodetic-grade receiver (SPAN receiver with NovAtel NOV-850 antenna) as a reference. The range errors were derived by applying the double-differenced method as discussed in Hu et al., (2023) and pre-measured lever arm. Figure 6 gives $L1$, $L2$ and $L3$ frequency code range temporal error characterization of Mosaic ×5 measurements. It can be noted that from 16:05 to 16:30, the measurement errors are noisy, indicating poor quality measurements in the urban environment. The statistics of the computed range errors for $L1$, $L2$ and $L3$ frequencies are represented in.

Table 3 $L1$ pseudorange errors standard deviation is the highest at 2.7 m as the signals on the $L1$ frequency are more susceptible to multipath.

The MRAKF results are compared with the existing method Yang and Gao (2006) which uses thresholds to apply the two-segment adaptive factor. The adaptive factor for the RAKF using thresholds is computed as shown in below.

$$\alpha = \begin{cases} 1 & \text{if } |r_i| \le c_0 \\ e^{-(|r_i|-c_0)} & \text{if } |r_i| > c_0 \end{cases} \tag{7}$$

In (7), $|r_i|$ is the learning statistic and c_0 is a constant derived by using the 95-percentile value from the distribution of innovation residuals. The learning statistic for the RAKF with thresholds used in this work for evaluation is standardized residuals. From here onwards, Yang (2010) and Yang and Gao (2006) method used for comparison will be referred to as RAKF method with thresholds.

Figure 7 describes the horizontal position error of the integrated solution with and without MRAKF enhancements and the RAKF method with thresholds. Hereafter, the variance component ratio-based MRAKF is referred to as method 1 and system innovations residual-based MRAKF is known as method 2 in all figures and discussions.

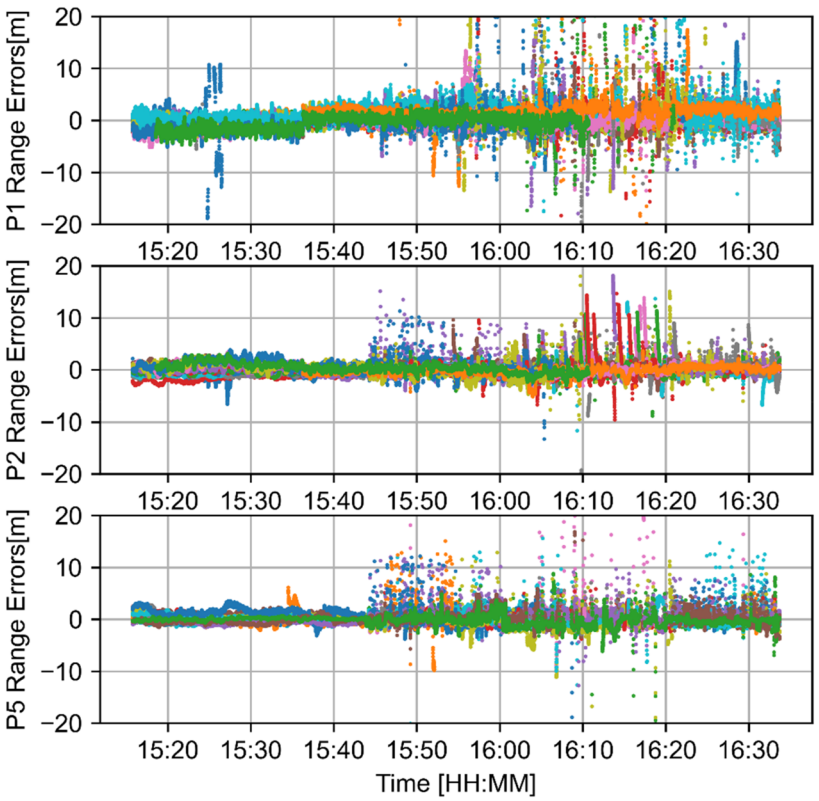

Fig. 6 Temporal range error characterization of Mosaic ×5 measurements (August 10, 2022) compared to the reference (SPAN) data for *L*1, *L*2 and *L*5 measurements

Table 3 Statistic for the temporal range errors of Mosaic ×5 data, August 10, 2022

Measurement type	Mean [m]	Standard deviation [m]
*L*1 pseudorange	0.01	2.7
*L*2 pseudorange	0.01	1.0
L5 pseudorange	0.1	1.0

In Fig. 7, there are two underpasses that the car passes; one is at 15:50 h and the other at 16:30 h. The data between time 16:05 h and 16:20 h were collected in an urban area. Figure 8 is a plot of the number of tracked satellites and PDOP. In the urban area, there is a drop in satellite count and an increase in PDOP corresponding to passage through the underpass and urban area. PDOP shoots up to as much as 20 when the number of measurements is insufficient to estimate all states.

In Fig. 7, when the car traverses the underpass at 15:50 h, the solution without enhancements and RAKF with thresholds diverge and the horizontal positioning error increases to one meter. Once satellites are tracked again after exiting the underpass, the PPP solution takes a few minutes to re-converge. A similar trend of the solution divergence is noticed when the car is traversing through the downtown area from 16:05 to 16:30 h. The solutions with enhancements, both

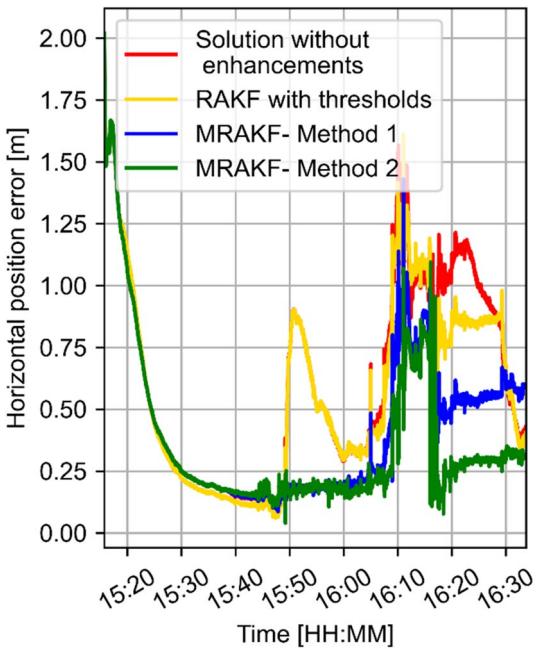

Fig. 7 Horizontal solution plot of August 10, 2022, data without enhancements and both the MRAKF methods

methods 1 and 2, impressively remain below 25 cm position accuracy even after passing the underpass at 15:30 h as MRAKF is applied at this time. The position accuracy below

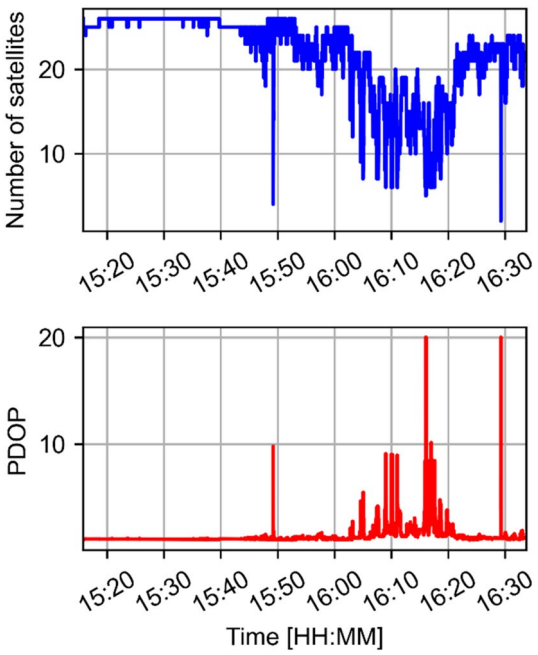

Fig. 8 Number of satellites and DOP for August 10, 2022 data

25 cm is maintained after the car travels through the underpass. In the case of the second underpass at 16:30 h, the position solution with MRAKF remains below the sub-meter positioning error. Method 2 performs better than method 1 in the urban area (16:05–16:20 h), as method 2 operates in the observation space and the indication of epochs with noisy and multipath prone measurements are flagged better than method 1, which operates in estimation space. When an outlier is detected in the observation space, the exclusion or deweighting of the measurement is easier. In case of the urban area (between 16:05 and 16:20 h), the available number of satellites varies between 15 and 5 several times. When consecutive epochs vary between over-determined and under-determined solutions, the PPP estimation process struggles to recover and converge as multiple measurements prone to multipath, noise, etc., are present in the urban area. The MRAKF solutions show a dramatic improvement of 38–55% in RMS when compared to the solution without RAKF enhancements.

Table 4 Horizontal error statistics for with and without enhancements for August 10, 2022 data

	Without RAKF	RAKF—with thresholds	MRAKF method 1	MRAKF method 2
Horizontal RMS [cm]	70	60	43	31
Percentage improvement	–	14%	38%	55%

Table 4 contains the summary of the overall RMS of the horizontal position error. Statistics include the horizontal position RMS for solution without enhancements, RAKF with thresholds, and MRAKF method 1 and method 2. The solution accuracy of RAKF with the thresholds method is 60 cm, which is a decimeter better than the solution without any enhancements. The horizontal position solution for method 2 performs 24% better than method 1. As the goal of this research is to apply MRAKF to maintain the accuracy of the position solution to below one meter throughout a route, it can be seen from Fig. 7 that the objective has been satisfied to a large extent.

Figure 9 is the representation of the adaptive factor α for RAKF with thresholds and both methods of MRAKF. It is quite evident from Fig. 9 that, while using RAKF method with thresholds, the adaptive factor is close to 1 in large number of epochs while MRAKF methods 1 and 2 are less than one in the time period 16:05–16:20. The underpass at 15:30 is not detected by RAKF with thresholds method resulting in no improvements in the underpass area (15:30) when compared to the solution without any enhancements. From the figure, it can be concluded that MRAKF method 1 gives higher priority to the GNSS receiver compared to MRAKF method 2. In a sky-obstructed environment, the key factor is to assign priority to the most reliable sensor. In this dataset, applying method 2 delivers higher position accuracy performance than method 1 as the learning statistic computation for method 2 results from information from observation space (system innovations). It is quite interesting to

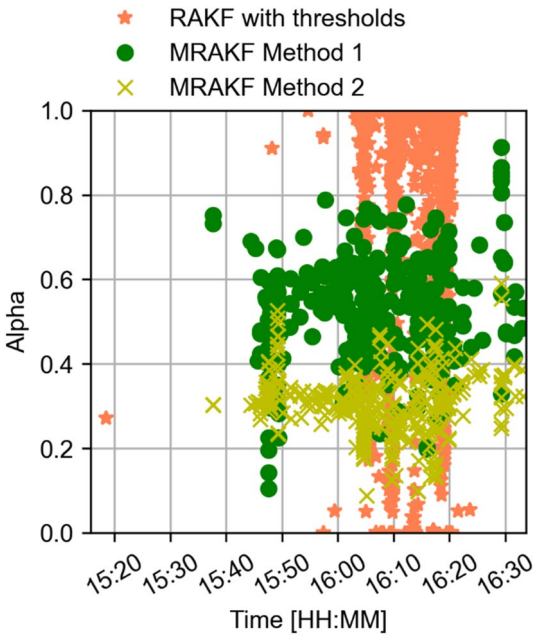

Fig. 9 Adaptive factor alpha plot for RAKF with thresholds, MRAKF method 1 and MRAKF method 2

study how the α adaptive factor varies based on the statistic chosen and how the adaptive factor affects the position solution. The adaptive factor computation is the key to the success of the MRAKF method, balancing the weight between the two sensors at the right times to achieve a lower position error. During the brief underpass outage, it can be noticed that the adaptive factor α for both methods 1 and 2 is close. Therefore, the position accuracy results from both methods are similar. As the car enters the urban area between 16:05 and 16:20 h, due to swiftly changing satellite numbers and measurements prone to multipath, noise, etc., adaptive factor α values computed by method 1 and method 2 are different. From Fig. 9, it is clear that the adaptive factor values are lower for method 2 compared method 1 in the urban area indicating that IMU is given higher priority while applying MRAKF, which in turn results in greater position accuracy in the case of method 2. In order not to draw conclusions based on one dataset, 5 other datasets were collected and performance was assessed.

Figure 10 is the RMS percentage improvement comparison of MRAKF two methods over the non-enhanced solution of different datasets collected in 2022. Table 5 is a list of datasets collected, length and environment conditions for

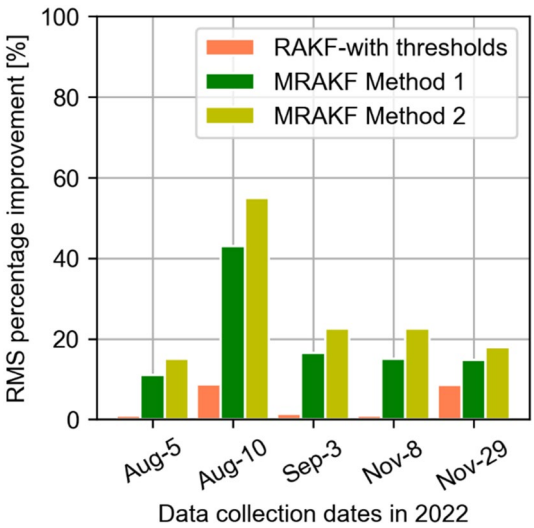

Fig. 10 Percentage improvement in horizontal RMS for RAKF with thresholds and MRAKF both methods when compared to no enhancements

corresponding data. The percentage improvement exhibited by MRAKF both methods is significant compared to the solution without any enhancements. RAKF method with thresholds does perform better when compared to the solution with no enhancements; however, the improvements are minimal when compared to improvements achieved with MRAKF method. Overall, the system innovations residual-based learning statistic (method 2) performs better than the position variance-based learning statistic (method 1) by 2–12%. Testing multiple datasets gives confidence that applying MRAKF to the urban data definitely provides improvements over not applying any kind of adaptive filtering techniques. MRAKF provides 6–46% better accuracy compared to RAKF with thresholds and 11–55% better accuracy performance when compared to solution without enhancements over multiple datasets. August 10, 2022 dataset was collected by spending more time in the urban areas compared to other datasets and was also driven during peak traffic hours. Therefore, applying MRAKF helps the datasets that have noisier data.

One of the reasons the system innovations method performs better is that the learning statistic for the system innovations-based method is formed with information from the observation space; therefore, it can go through screening to flag outlier measurements. In the position variance method, not all the abnormalities from the observation space may be reflected in the estimation space. Therefore, there can be indications from the observation space that may be missed in the current estimation space. However, the missed observation outliers will cause larger position errors in the following epochs. Another reason the system innovations-based method performs with higher position estimation accuracy is that the position variance is scaled with the system innovations variance in method 1. If both the position variance and the system innovations variance are high, the learning statistic may not give any indication of adaptiveness. As method 1 needs the change in position information to invoke the adaptiveness, the computation cycles increase. On the other hand, method 2's adaptiveness can be applied when performing the estimation without requiring re-running the estimation portion of EKF.

Figure 11 shows the percentage of time when the horizontal position error is less than one meter for the solution

Table 5 Datasets collected and related information details

Date	Length of data [min]	Environment conditions
August 5, 2022	50	20 min data were collected in obstructed environment, medium traffic
August 10, 2022	70	Over half an hour spent in obstructed environment during peak rush hour
September 3, 2022	45	20 min data were collected in obstructed environment, medium traffic
November 8, 2022	55	Less than 20 min data in obstructed environment, light traffic
November 29, 2022	70	Over half an hour data in obstructed environment, medium to light traffic

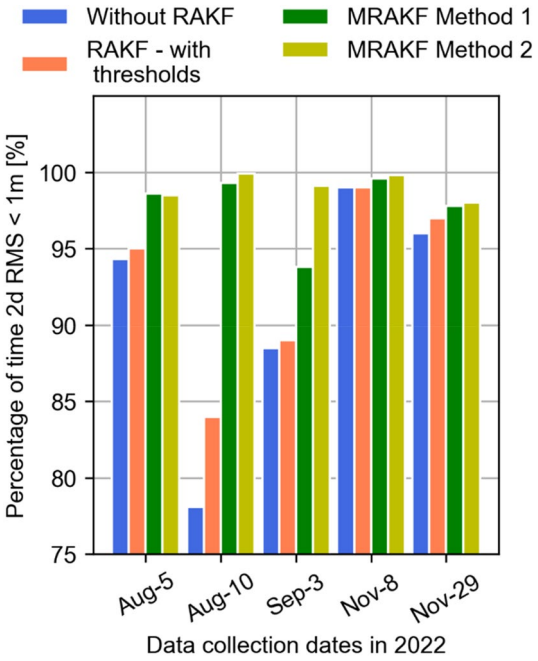

Fig. 11 Percentage of time when horizontal position error is less than one meter for different datasets

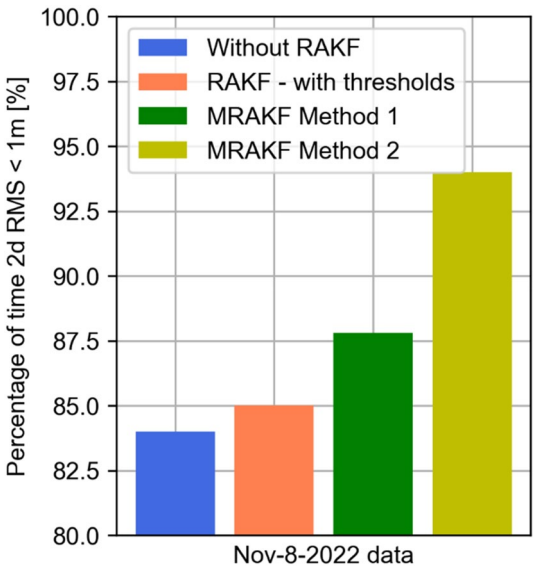

Fig. 12 Percentage improvement for Nov-8-2022 data in horizontal RMS with RAKF with thresholds and MRAKF both methods when compared to no enhancements only in urban areas

without any enhancement and the solutions with MRAKF (methods 1 and 2) technique applied. When RAKF with thresholds is applied, there are no significant improvements to the percentage of time when the horizontal position remains below a meter. It is evident that applying the MRAKF method clearly improves the amount of time when the horizontal position solution error remains less than one meter. The percentage of time when horizontal error is less than one meter by applying MRAKF method 1 or 2 is 2–22% better when compared to when no enhancements are applied. The November 8, 2022 dataset was collected in the nighttime; therefore, the position error did not have many spikes due to vehicular traffic. The largest improvements were seen in the most obstructed dataset (August 10, 2022), the MRAKF enhancements provide the largest percentage improvements.

As the November 8, 2022 data were collected at nighttime and the overall performance without any enhancements is as good as 96% below one meter accuracy, an attempt to understand the accuracy performance in the urban environment alone is made in Fig. 12. From Fig. 12, it is evident that when no enhancements are applied, the solution accuracy better than one meter occurs only 84% of the time. When the RAKF method with thresholds is applied, it can be noticed that there is a solution accuracy improvement of 2.5% compared to no enhancements in the urban areas. However, by applying methods 1 and 2 MRAKF enhancements, there is an improvement in the percentage of time when the position solution accuracy remains below one meter. When MRAKF method 1 is applied, the percentage of time the solution is below one meter is 87% and with method 2 it goes up to 94%. The change in percentage improvement by 4–10% is quite significant for the urban environment with low-cost equipment.

Research work conducted by Yang and Gao (2005) achieved a 60% horizontal accuracy performance improvement in RTK mode for flight data when RAKF was used in its traditional form with the state discrepancy-based statistic and exponential function for the adaptive factor computation. These results cannot be directly compared with the current research work as the processing technique used is RTK mode, along with a high-performance GNSS receiver and antenna for data collection and the application is different from the one targeted by the current work. To perform the same data analysis with an existing method, RAKF with thresholds method involving adaptiveness only for the dynamic model has been assessed in this work using Yang and Gao (2005) method.

Figures 7, 8, 9, 10, 11 and 12 show that applying MRAKF significantly impacts low-cost sensors to achieve the objective of this research, which is to maintain position error below one meter as much as possible. The proposed MRAKF method based on slope of the satellite count and the number of measurements available achieves a significant improvement to the results. Application of such software enhancements to improve the results is a significant step toward using low-cost sensors for navigation compared to high-precision sensors that are expensive, and bulky sensors.

Conclusions and future work

Adaptive filtering becomes mandatory while using low-cost equipment to achieve accurate, continuous and precise navigation solutions in urban environments (Vana 2021, 2023). In a traditional RAKF, empirical values are used to determine when the RAKF filter is to be invoked. In this research, the dependence on the empirical values has been avoided by applying adaptiveness and detecting the rise in the incoming satellites after a partial or complete GNSS outage. Removing the dependency on the empirical value is a significant development and contributions of this work. Two learning statistics were examined, namely: (1) variance component method based on change in position and innovation method and (2) system innovations-based method.

The modified-RAKF method was discussed, and the results are quite positive. When MRAKF is used, it is shown that the position is below a meter most of the time—close to 98–99%. A dm-level RMS was maintained throughout the data that were tested. To compare the solution accuracy, RAKF with thresholds method, MRAKF method 1 and method 2, performed 14%, 38% and 55% better when compared to the solution with no enhancements. Furthermore, to make a stronger conclusive remark, multiple datasets were tested, and the urban area data proved to perform better when MRAKF is applied than when no adaptiveness is applied. Method 2 performs 10–30% better than the method 1, as the measurement domain can detect measurement outliers earlier than the position domain. These results prove that the MRAKF proposed in this research work is promising to achieve continuous, precise and accurate navigation solutions in urban environments using tightly coupled TF-GNSS-PPP and MEMS-IMU. There is no previous research with which the results from the current research can be directly compared, as there has been no work done in the low-cost sensor area using RAKF to make it independent of the empirical boundaries to detect the need to apply adaptiveness in the case of Kalman gain.

As part of future work, other GNSS and IMU sensor data with different GNSS data rates need to be collected and tested to validate the proposed modification to the RAKF algorithm. The reconvergence issue can be dealt with as a next step by applying ionosphere constraining and PPP-AR (Naciri et al. 2021).

Ethics approval

Not applicable.

Acknowledgements The authors would like to thank the Natural Sciences and Engineering Research Council (NSERC) and York University for providing funding for this research and the Centre National d'Etudes Spatiales (CNES) for data. The authors would also like to thank GNSS Lab, York University members for data collection and other supportive activities.

Author contribution SV performed the processing and analysis and wrote the manuscript. SB led the development of the paper and provided advice and guidance for the experimental design, analysis and paper writing, and reviewed and edited the manuscript. Both authors reviewed the paper and agreed to the submitted version.

Funding Funding for this research was provided by the National Science and Engineering Research Council of Canada (NSERC) and York University.

Data availability The data used in this research were collected by sensors owned by GNSS Lab, York University, Canada. The data are not available publicly currently. If a person or a party is interested in using the data, they can reach out to the corresponding author.

Declarations

Competing interests The authors declare no competing interests.

References

Aggrey J (2018) Assessment of global and regional ionospheric corrections in multi-GNSS PPP. In: Proceedings of ION GNSS+ 2018, Institute of Navigation , Miami, Florida, September 2018, pp 3967–3981. https://doi.org/10.33012/2018.16079

Brown RG, Hwang PY (1997) Introduction to random signals and applied Kalman filtering: With MATLAB exercises and solutions. Wiley, New York

Cai Q, Yang G, Song N, Pan J, Liu Y (2017) An Online Smoothing Method Based on Reverse Navigationfor ZUPT-Aided INSs. J Navigation 70(2):342–358. https://doi.org/10.1017/S0373463316000667

Choy S, Bisnath S, Rizos C (2016) Uncovering common misconceptions in GNSS precise point positioning and its future prospect. GPS Solut 21:13–22. https://doi.org/10.1007/s10291-016-0545-x

Eueler H-J, Goad CC (1991) On optimal filtering of GPS dual frequency observations without using orbitinformation. Bull Géodésique 65(2):130–143. https://doi.org/10.1007/BF00806368

Elmezayen A, El-Rabbany A (2021) Real-time GNSS precise point positioning using improved robust adaptive Kalman filter. Surv Rev 53(381):528–542. https://doi.org/10.1080/00396265.2020.1846361

Farrell J (2008) Aided navigation: GPS with high rate sensors. McGraw-Hill, Inc.

Groves PD (2013) Principles of GNSS, inertial, and multisensor integrated navigation systems. Artech house

Hofmann-Wellenhof B, Lichtenegger H, Wasle E (2007) GNSS–global navigation satellite systems: GPS,GLONASS, Galileo, and more. Springer Science & Business Media

Hide C, Moore T, Smith M (2003) Adaptive Kalman filtering for low-cost INS/GPS. J Navig 56(01):143–152. https://doi.org/10.1017/S0373463302002151

Lotfy A, Abdelfatah M, El-Fiky G (2022) Improving the performance of GNSS precise point positioning by developed robust adaptive Kalman filter. Egypt J Remote Sens Space Sci 25(4):919–928. https://doi.org/10.1016/j.ejrs.2022.09.005

Li Y, Shen Y (2011) GPS/INS tightly coupled integration based on adaptive robust kalman filter. In: Proceedings of the 24th

international technical meeting of the satellite division of the institute of navigation (IONGNSS 2011), pp 2271–2279
Magill D (1965) Optimal adaptive estimation of sampled stochastic processes. IEEE Trans Autom Control 10(4):434–439. https://doi.org/10.1109/TAC.1965.1098191
Naciri N, Bisnath S (2021) An uncombined triple-frequency user implementation of the decoupled clock modelfor PPP-AR. J Geodesy 95(5):1–17. https://doi.org/10.1007/s00190-021-01510-y
Naciri N, Vana S, Seepersad G, Bisnath S (2021) Rapid position initialization for automated automotive applications. In: Proceeding of ION GNSS+ 2021, Institute of Navigation , St. Louis, Missouri, September 2021, pp 2718–2732. https://doi.org/10.33012/2021.17959
Niehsen, W. (2004). Adaptive Kalman Filtering based on Matched Filtering of the Innovations Sequence. In: Proceedings of the 7th International Conference on Information Fusion, Stockholm, Sweeden. 2004, 362–369.
Vana S, Bisnath S (2020) Enhancing navigation in difficult environments with low-cost, dual-frequency GNSS PPP and MEMS IMU. In: International association of geodesy symposia, vol 152. Springer, Berlin Heidelberg. https://doi.org/10.1007/1345_2020_118
Vana S, Naciri N, Bisnath S (2020) Benefits of motion constraining for robust, low-cost, dual-frequency GNSS PPP+MEMS IMU navigation. In: IEEE/ION PLANS 2020, Portland, OR, USA, 2020, pp 1093-1103. https://doi.org/10.1109/PLANS46316.2020.9109982
Vana S (2021) Low-cost, triple-frequency multi-GNSS PPP and MEMS IMU integration for continuous navigation in urban environments. In: Proceedings of ION GNSS+ 2021, Institute of Navigation , St. Louis, Missouri, September 2021, pp 3234–3249. https://doi.org/10.33012/2021.18093
Vana S (2023) Continuous urban navigation with next- generation, mass market navigation sensors and adaptive filtering. Doctoral dissertation, York University.
Wu Y, Chen S, Yin T (2022) GNSS/INS tightly coupled navigation with robust adaptive extended kalman filter. Int J Auto Technol 23(6):1639–1649. https://doi.org/10.1007/s12239-022-0142-7
Yang Y (2010) Adaptively robust Kalman filters with applications in navigation. In: Xu G (ed) Sciences of geodesy—I. Springer, Berlin Heidelberg, pp 49–82. https://doi.org/10.1007/978-3-642-11741-1_2
Yang Y, Cui X (2008) Adaptively robust filter with multi adaptive factors. Surv Rev 40(309):260–270. https://doi.org/10.1179/003962608X325330
Yang Y, Gao W (2005) Comparison of adaptive factors in Kalman filters on navigation results. J Navig 58:471–478. https://doi.org/10.1017/S0373463305003292
Yang Y, Gao W (2006) An optimal adaptive Kalman filter. J Geodesy 80(4):177–183. https://doi.org/10.1007/s00190-006-0041-0
Yang Y, He H, Xu G (2001) Adaptively robust filtering for kinematic geodetic positioning. J Geodesy 75(2):109–116. https://doi.org/10.1007/s001900000157
Yi D, Bisnath S, Naciri N, Vana S (2021) Effects of ionospheric constraints in precise point positioning processing of geodetic, low-cost and smartphone GNSS measurements. Measurement 183:109887. https://doi.org/10.1016/j.measurement.2021.109887
Zhou Z, Li Y, Rizos C, Shen Y (2009) A robust integration of GPS and MEMS-INS through trajectory-constrained adaptive Kalman filtering. In: Proceedings of ION ITM 2009, Savannah, GA, September 2009, pp 995–1003
Zumberge JF, Heflin MB, Jefferson DC, Watkins MM, Webb FH (1997) Precise point positioning for the efficient and robust analysis of GPS data from large networks. J Geophys Res Solid Earth (1978–2012) 102(B3):5005–5017. https://doi.org/10.1029/96JB03860

Sudha Vana is working as High Precision Research Engineer at Rx Networks, Inc. She received her Ph.D. from York University, Toronto, Canada, in the Earth and Space Science and Engineering Department. She holds a master's degree in Electrical Engineering from Ohio University. She has worked for Volvo India and Broadcom Inc. in the past. Her research interests include low-cost GNSS-PPP and MEMS-IMU sensor fusion in urban environments.

Sunil Bisnath is a Professor in the Earth and Space Science and Engineering Department at York University, Toronto, Canada. He received his Ph.D. in Geodesy and Geomatics Engineering from the University of New Brunswick. For 30 years, he has been actively researching GNSS processing algorithms for positioning and navigation applications.